Limb Correction Effects on TIROS-N Microwave Sounding Unit Observations

THOMAS L. KOEHLER

Marine Physical Laboratory, Scripps Institution of Oceanography, University of California, San Diego, San Diego, California

(Manuscript received 19 May 1988, in final form 3 December 1988)

ABSTRACT

Evaluations of limb-corrected brightness temperatures computed by NESDIS from TIROS-N MSU observed brightness temperatures are presented. Observed brightness temperatures both before and after limb correction are compared to simulated brightness temperatures derived from conventional radiosonde measurements.

Results suggest a left-to-right bias in the limb-corrected MSU data, with the left side colder than the right side. The uncorrected MSU brightness temperatures can be more accurately simulated than those available after the limb correction technique is applied. Incorporating the actual MSU antenna patterns into the simulations removes most of the scan angle dependence in the bias differences.

1. Introduction

The accuracy of the satellite-derived temperature profiles produced operationally by the National Environmental Satellite Data and Information Service (NESDIS) during the Global Weather Experiment (GWE) has been the topic of many studies, including Phillips et al. (1979), Schlatter (1981), Gruber and Watkins (1982), and Koehler et al. (1983). Errors in satellite retrievals arise from several sources, including radiance measurement errors, errors in the retrieval algorithm, and basic physical limitations in the determination of vertical temperature profiles from satellite radiance measurements. Koehler et al. (1987) focused on alternatives to two aspects of the operational NESDIS retrieval technique employed during the Global Weather Experiment (GWE). They found little improvement in the accuracy of the retrievals from using a physical retrieval algorithm instead of the operational statistical method, or from compositing the radiance information over 3×3 infrared field-of-view arrays, instead of the 9×7 arrays used in the operational method. LeMarshall and Schreiner (1985) suggest that limb correction of the basic radiance data may contribute to satellite sounding errors. The study presented here examines the accuracy of the limb correction procedure for the microwave channels by comparing observed brightness temperatures from the Microwave Sounding Unit (MSU) aboard TIROS-N, both before and after limb correction, to simulated brightness temperatures derived from conventional temperature measurements.

Corresponding author address: Dr. Thomas L. Koehler, Marine Physical Laboratory, Scripps Institution of Oceanography, University of California, San Diego, San Diego, CA 92152.

Accurate MSU brightness temperatures are crucial in several steps in the operational retrieval algorithm, such as detecting cloud contamination in the infrared measurements, and determining the retrieval coefficients to be applied in the statistical retrieval algorithms. Thus, inaccuracies introduced by the microwave limb correction procedure could be amplified during subsequent steps in the NESDIS retrieval process.

2. A description of MSU measurements

The MSU carried aboard TIROS-N series of satellites consisted of two 10.2 cm antenna systems that make measurements at four frequencies (50.30, 53.74, 54.96 and 57.95 GHz). The antenna scans from left to right in eleven 9.47° steps across the orbital track. Figure 1 illustrates the distribution of the center points of the microwave observations from one orbit over the central United States. The numbering system for identifying the scan positions used in this paper is also shown, with position 6 corresponding to nadir, and positions 1 and 11 corresponding to the extreme scan angles of −47.35° and +47.35° respectively. Microwave measurements are volumetric in nature, with most of the energy coming from a conical volume whose intersection at the earth's surface forms a circle at nadir with a diameter of approximately 110 km, and an ellipse at the extreme angles with major and minor axes of 325 and 179 km, respectively. As noted by Grody (1983), the wavelength being measured (0.5 cm) is not negligible compared to the instrument dimensions. Thus, the relative response of an MSU channel over its field of view is defined by the diffraction pattern of its antenna. A small portion of the total measured energy emanates from outside the nominal field-of-view due to side lobes in the diffraction pattern.

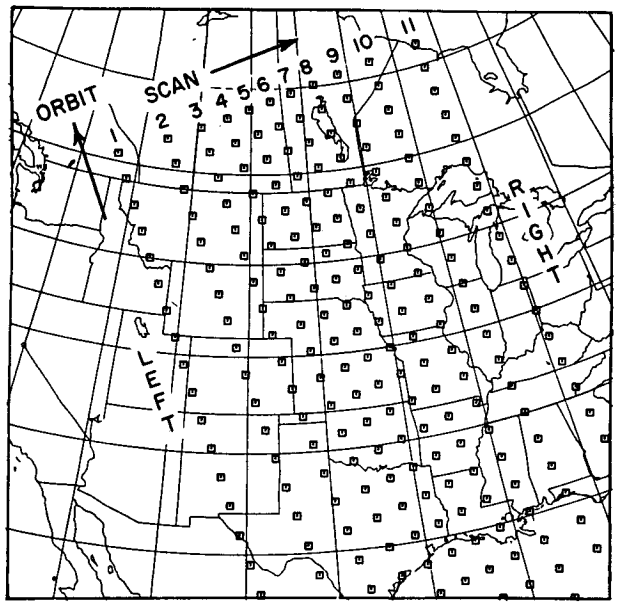

FIG. 1. MSU scan locations for 2100 UTC 6 January 1980. The numbering system for the different scan positions is shown, with 1 on the left and 11 on the right. The arrow is drawn to the left of the pass points in the direction the satellite is progressing along the orbit.

The energy measured by a microwave sensor aboard an orbiting satellite is related to the vertical temperature distribution through the radiative transfer equation. The version of this equation valid for the microwave frequencies is

$$T_B(\nu) = \tau(p_s)T_s\epsilon_s + \tau(p_s)(1-\epsilon_s)\int_0^{p_s} T(p)\frac{\partial\tau'(p)}{\partial \ln p} \times d\ln p + \int_{p_s}^{0} T(p)\frac{\partial\tau(p)}{\partial \ln p}\,d\ln p, \quad (1)$$

where

$$\tau(p) = \exp\left[-\sec\theta\int_0^p \alpha(\nu, p, T)dp\right] \quad (2)$$

and

$$\tau'(p) = \tau(p_s)/\tau(p). \quad (3)$$

In these expressions, T_B is the brightness temperature at a specified frequency (ν), T is the temperature that varies as a function of pressure (p), T_s is the surface radiating temperature, ϵ_s is the surface emissivity, τ is the atmospheric transmittance of energy radiated toward space at a given pressure, τ' is the transmittance of energy radiated toward the earth's surface, and α is the atmospheric absorption coefficient at a specified frequency that varies as a function of pressure and temperature. The first term on the right in (1) represents energy emitted by the earth's surface that reaches the satellite, the second is the downward-directed atmospheric emission reflected back toward the satellite by the earth's surface, and the final term represents direct upwelling atmospheric radiation.

The dependence of brightness temperature measurements on scan angle enters through the $\sec\theta$ term in (2), where θ is the local zenith angle of the satellite measured from the earth's surface. [Koehler (1986a) presents a method for determining the local zenith angle within the MSU footprint given the scan angle and the position within the sampled volume.] At greater scan angles, the upwelling energy must pass through a longer path in the atmosphere, which displaces the weighting function ($-\partial\tau/\partial \ln p$) higher into the atmosphere, as illustrated in Grody (1983). This causes brightness temperatures at the edge of the orbit to be nearly 12 K colder than at the center for the lower tropospheric 53.74 GHz channel (Ch. 2), and 6.5 K colder for the upper tropospheric 54.96 GHz channel (Ch. 3) using the standard atmospheric temperature profile. This is the so-called "limb darkening" effect.

3. The operational limb correction procedure

The NESDIS operational retrieval technique used during the GWE was designed to use brightness temperatures which were corrected for the effect of scan angle. The limb correction procedure for the MSU channels corrects not only for limb effects, but also for several other factors that affect the actual microwave measurements, including precipitating clouds, variable surface emissivity, and side lobes in the antenna pattern. While the microwave measurements are relatively insensitive to the presence of cloud droplets, precipitation, especially convective precipitation, can affect the measurements, as shown for example in Grody (1983). Also, surface emissivities for the microwave channels are more variable than infrared emissivities, with values varying from 0.5 over water to nearly 1.0 over dry land. Finally, as mentioned earlier, antenna response patterns for the microwave instruments display side lobes produced by diffraction properties of the instrument. The antenna pattern applied by NESDIS in determining the TIROS-N limb correction coefficients is presented in the top of Fig. 2. This idealized pattern was based on the antenna response of Scanning Microwave Spectrometer (SCAMS) carried aboard the previous generation Nimbus-6 satellite (Woolf 1984, personal communication). The labels in Fig. 2 are the logarithm of the antenna response, and distance from the intersection of the axes corresponds to the angular distance from the central axis of the conical volume being sampled. Thus, responses greater than 10^{-1} in the idealized pattern are confined mostly within a 6° cone centered about an axis oriented at a given scan angle, and signal responses greater than 10^{-4} are present at 20°. At far scan angles, some of the measured radiance comes from space instead of the earth's atmo-

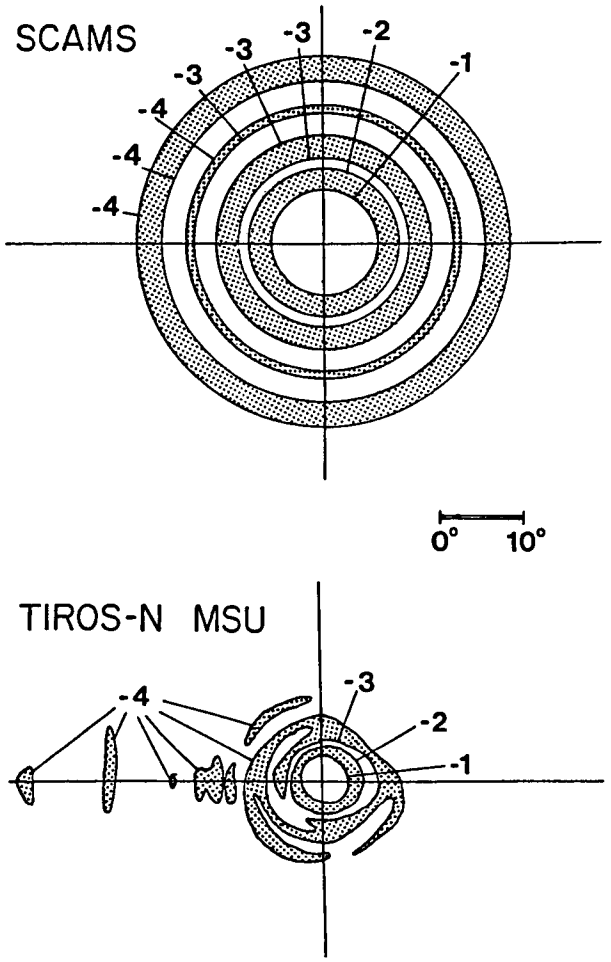

FIG. 2. Microwave antenna response functions for the idealized footprint used in the development of the TIROS-N limb correction coefficients (SCAMS) and the actual TIROS-N response function for Ch. 2 at nadir. The contour labels refer to the logarithm of the instrument response, and horizontal distance is angular distance from the center of the observing cone.

sphere, an effect that will be examined more closely in a later section.

The NESDIS MSU limb correction technique is described briefly in Werbowetzki (1981). In this technique, statistical coefficients are applied to the four measured brightness temperatures at a particular scan location to determine corrections to these observations, such that they become equivalent to observations at zero scan angle with a surface emissivity of one. The limb correction coefficients were developed from simulated radiances determined using (1) for a global sample of 100 atmospheric temperature and moisture profiles. Separate sets of coefficients were derived over both land and water. "Observations" were simulated by incorporating the effects of scan angle, antenna pattern, variable surface emissivity, and, over land, the effects of precipitating clouds into the appropriate terms in (1). The antenna pattern was incorporated by weighting transmittances at selected locations within the footprint by their associated antenna responses, to produce an effective transmittance for each scan location. A set of "limb-corrected" brightness temperatures were then computed using zero scan angle, a unit emissivity and no side lobes. A stepwise regression was then performed, relating the observed brightness temperatures for each of the four MSU channels to limb-corrected minus observed differences for a particular channel.

The first step in the limb correction of real MSU measurements is to determine whether the observations are over land or water, as indicated by the geographical position of the center of the microwave footprint. The appropriate regression coefficients for the given scan angle are then applied to the MSU observations to estimate corrections that are then added to the original data. The accuracy of the NESDIS limb correction procedure for TIROS-N measurements is evaluated in this paper by comparing observed MSU brightness temperatures (both before and after limb correction) to simulated values based on conventional radiosonde data. The following section describes the significant features of the simulation procedure.

4. Description of the brightness temperature simulations

The brightness temperature evaluations in this study focus on four orbital segments over the central United States and southern Canada on 5–6 January 1980. This region has reasonable conventional data coverage, and the same period was studied in previous satellite retrieval evaluations (Koehler et al. 1983, and Koehler et al. 1987). Simulated brightness temperatures were derived for the two MSU tropospheric sounding channels, Ch. 2 and Ch. 3.

Two types of simulated brightness temperatures were determined for the evaluations: angle dependent values that include the effects of scan angle and variable surface emissivity, and limb-corrected values assuming a zero scan angle and a unit surface emissivity at every scan position. A finite difference form of the radiative transfer equation (1) was employed, which required atmospheric temperature estimates and transmittance coefficients at the 40 isobaric levels from 1000 to 0.1 mb used in the standard NESDIS retrieval algorithms. Estimates of the surface pressure, skin temperature and surface emissivity at each scan location were also needed.

Temperatures for the 21 tropospheric levels from 1000 to 100 mb were interpolated in time and space to the MSU observation location from horizontal analyses of temperature derived from conventional radiosonde observations (see Koehler 1986b). Temperatures at and above 50 mb were taken from the regional climatology described in Koehler and Seman (1986). An adjustment based on the difference between the observed and climatological temperatures at 100 mb

was made to the climatological temperatures at 85 and 70 mb, to avoid an abrupt discontinuity between the conventional and the climatological values. (See Koehler 1986a.) Surface pressure was determined hydrostatically using the collocated observed temperatures and 1000 mb height, and a terrain elevation for the center of the microwave footprint. The skin temperature was set equal to the surface air temperature, and the surface emissivity was estimated from Ch. 1 in a manner described in Koehler (1986a). The standard NESDIS transmittance coefficients presented in Weinreb et al. (1981) were employed. Examples of observed and simulated MSU brightness temperature analyses from a limb-corrected dataset are given in Fig. 3.

There are several possible sources for the differences between observed and simulated brightness temperatures. The most obvious source is measurement error by the MSU instrument, which should be random in nature, and has been estimated to be about 0.2 K for Chs. 2 and 3. The limb correction procedure provides another observational source of error. Potential sources of error in the brightness temperature simulations include measurement errors in the original radiosonde observations; analysis errors from transferring these temperatures to a uniform grid; errors in the collocation procedure to the MSU scan location; the use of climatological data above 100 mb; possible limitations in modeling the transmittance functions; and ineffective treatment of the instrument side lobes. It is impossible to identify the exact proportion of each error sources in any given observed-minus-simulated difference. Some insight into the sensitivity of several of these components is gained, however, from the comparisons that follow.

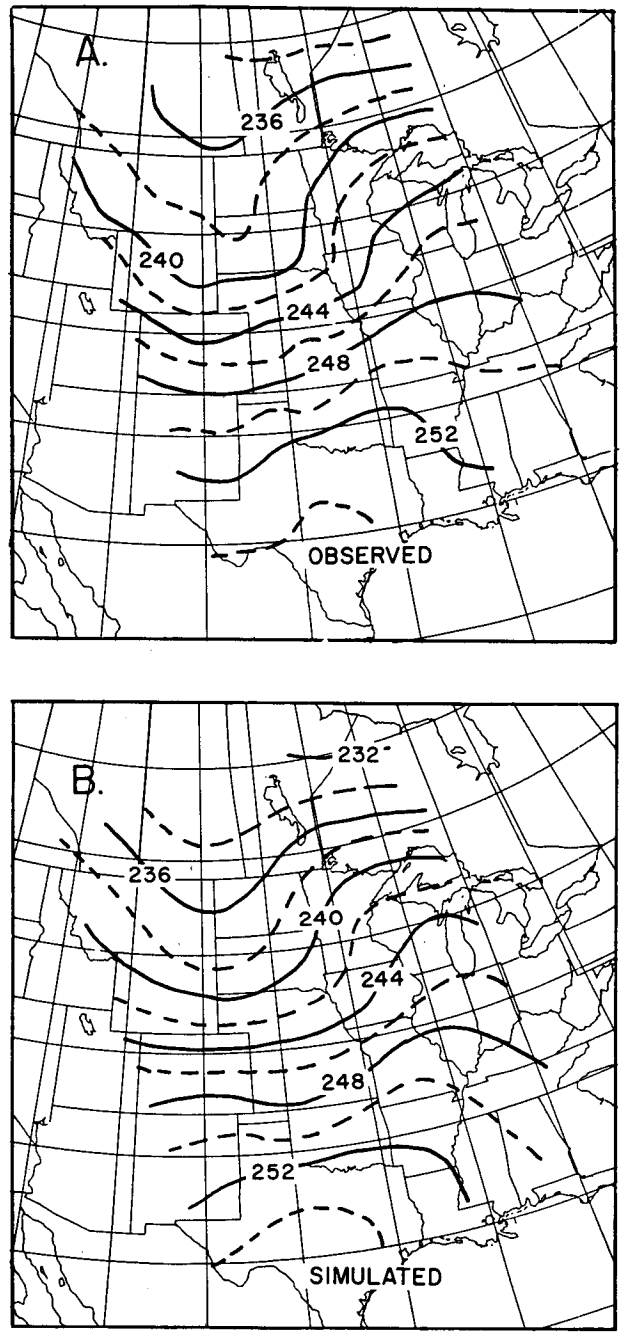

FIG. 3. Limb-corrected (a) observed and (b) simulated brightness temperatures (K) for TIROS-N MSU Ch. 2 at 2100 UTC 6 January 1980.

5. Evaluation of the limb-corrected data

Map analyses of the differences between the limb-corrected MSU observations and simulated brightness temperatures derived assuming zero scan angle and unit surface emissivity for MSU Ch. 2 are shown in Fig. 4. Four orbital segments separated in time by about 12 hours over the central United States and southern Canada are presented. The arrows on the left side of the orbit indicate the direction of the orbital path. The 0900 UTC orbits are descending (southward moving) orbits, while the 2100 UTC orbits are ascending (northward moving) orbits. Note also that negative differences are shaded, indicating areas where the limb-corrected observations are colder than the simulated values.

Two consistent patterns emerge from the results from this channel which peaks near 625 mb at nadir. First, large positive differences appear in the northern parts of all four orbits where locally cold air is indicated in the conventional 850 mb analyses (Fig. 5). Other large positive differences are also found on the right edge of the orbits (facing the direction of orbital motion). The largest negative differences are on the left side of the orbits, displaced one or two scan positions in from the left edge, with negative values exceeding 2.0 K in magnitude found over the Rockies at 2100 UTC 5 January. Note also the strong gradient in brightness temperature differences extending from central Wyoming northward through Montana. The orientation of the difference isotherms corresponds well

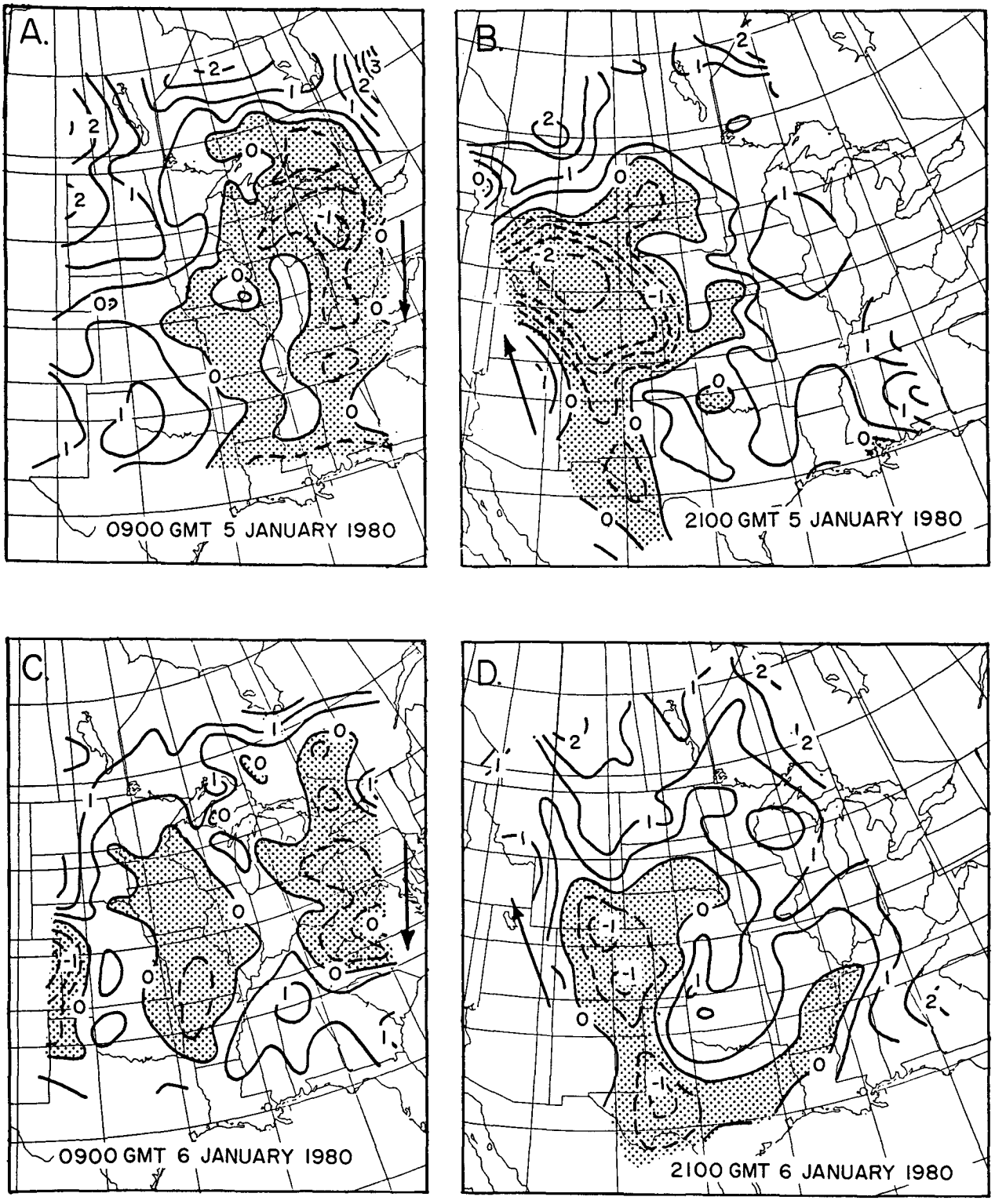

FIG. 4. Differences between the limb-corrected observed brightness temperatures and their simulated counterparts (K) for four orbits. Negative differences are shaded, and indicate regions where the simulated values exceed the observed values.

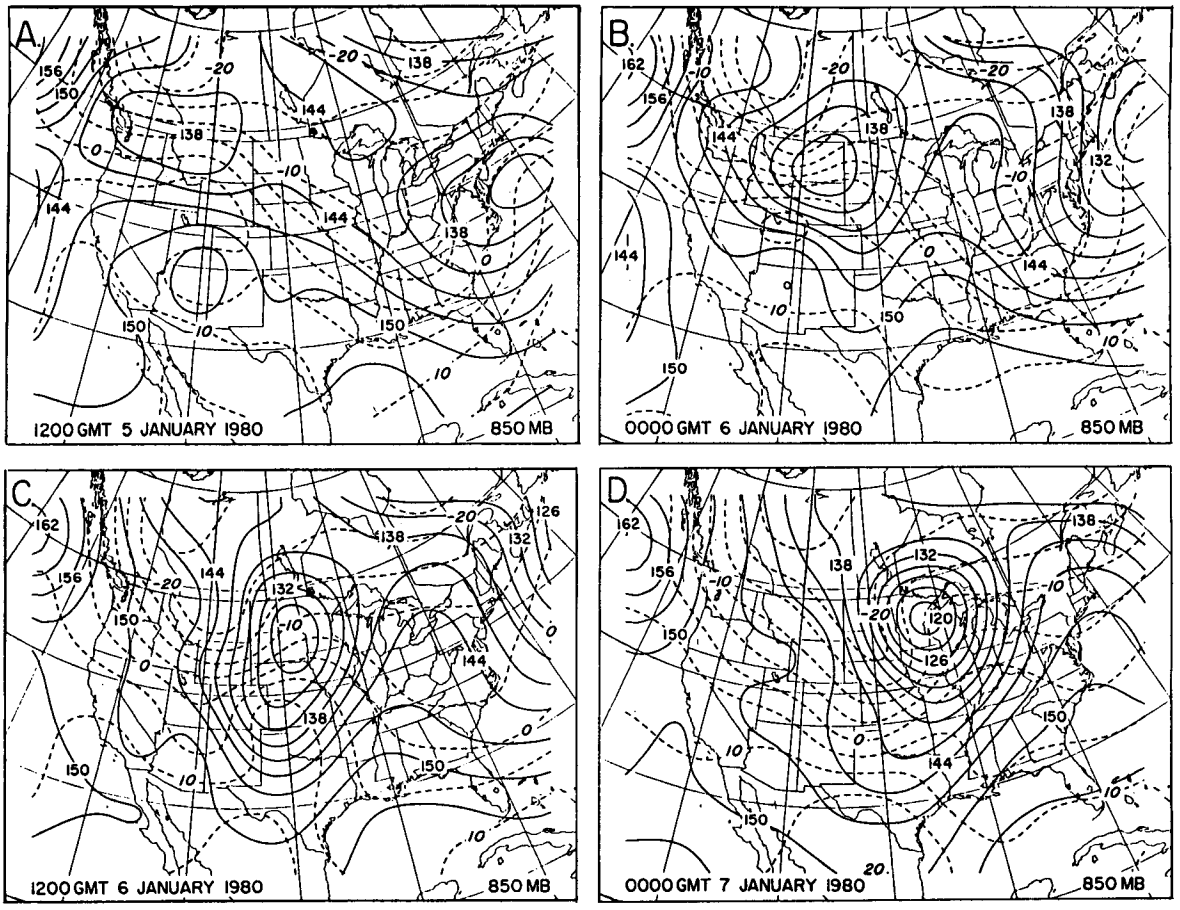

FIG. 5. 850 mb height (solid, dam) and temperature (dashed, °C) analyses for the four radiosonde ascent times nearest the satellite overpass times.

with the isotherm orientation on the 1200 UTC 5 January 850 mb chart (Fig. 6a). A similar orientation is found over the northern plains 24 hours later. While the effects of water vapor, clouds and precipitation were not fully considered in the simulation, the consistent brightness temperature difference patterns just noted bore little resemblance to the cloud and precipitation patterns (in Koehler 1986a). The results in Fig. 4 suggest a possible scan angle dependence in the observed-minus-simulated differences.

Statistical comparisons were prepared as a function of scan position to better detect possible scan angle dependence. Figure 6 summarizes the statistics in the form of biases (means) and standard deviations of the differences for both Chs. 2 and 3. The standard deviations provide a good measure of the variability of the differences within a particular scan position, and will be affected by both random measurement errors, and by systematic differences such as the presence of large positive values in the northern portion of the orbits noted in the results from Ch. 2. Separate computations were made for the ascending and descending orbits.

The bias values are generally positive for both channels except for position 2 of Ch. 2. Some left-to-right asymmetry is evident, with values on the right edge exceeding those on the left edge. It also appears that the limb correction is overcorrecting the original brightness temperatures, since biases at the outer scan locations are greater than those near the center. This is particularly true in Ch. 2, where the biases are at least 0.5 K greater in the outer scan positions (1 and 11) when compared to adjacent positions. Since the left side of the orbit is over the eastern United States for the 0900 UTC orbits, and over the Rockies at 2100 UTC, the likelihood that the left-to-right asymmetries are due to the synoptic situation is relatively small. As might be expected, the standard deviations for Ch. 2 in the low troposphere are substantially greater for the positions over the Rockies, primarily on the left side of the 2100 UTC ascending orbits. The effect of terrain is considerably less important for Ch. 3, which peaks near 275 mb at nadir. In summary, the limb-corrected brightness temperature difference bias statistics indicate a left-to-right asymmetry in the MSU observations and suggest overcorrection of the original brightness temperature measurements at the outer scan positions.

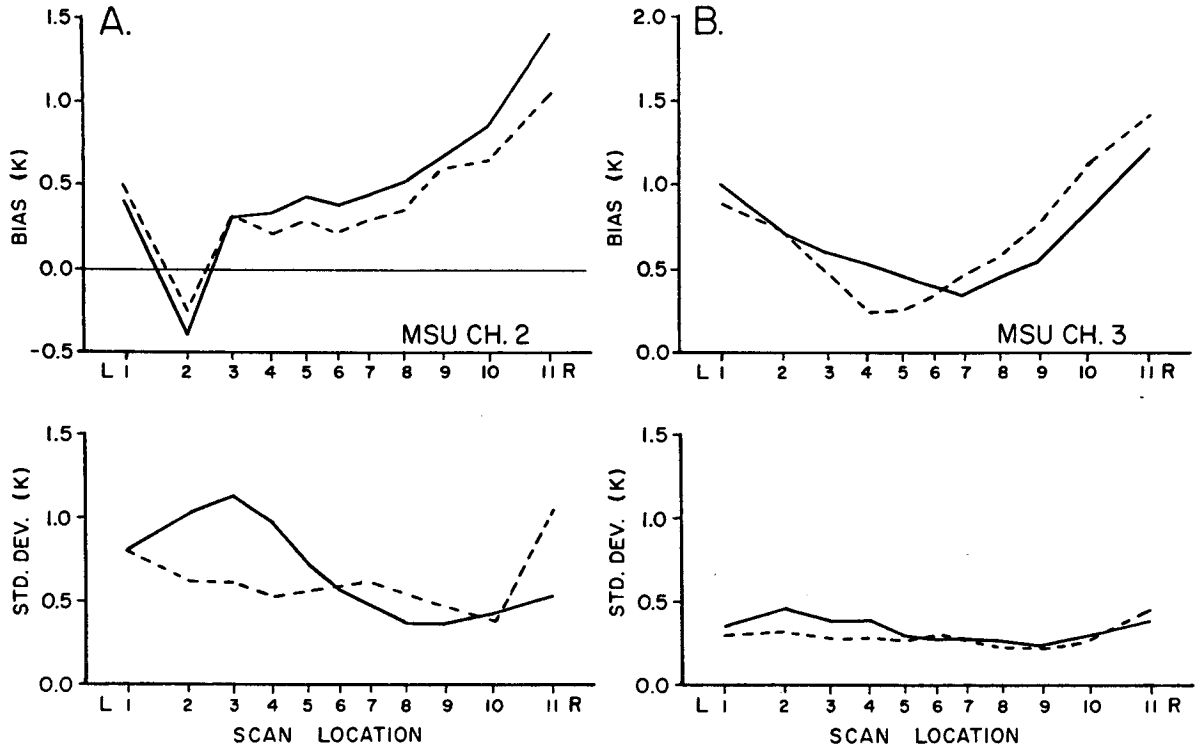

FIG. 6. Bias and standard deviation statistics for the limb-corrected observed-minus-simulated differences as a function of scan position. The dashed line is for the descending (0900 UTC) orbits and the solid line is for the ascending (2100 UTC) orbits.

Standard deviations of the differences are nearly twice as large for Ch. 2 compared to Ch. 3, and increase for Ch. 2 in regions with high terrain.

6. Results without limb correction

To accurately simulate the measured brightness temperatures without limb correction, the effects of varying the scan angle and surface emissivity, and the presence of instrument side lobes must now be adequately modeled. Before describing the side lobe correction technique and the resulting computations, some background on how side lobes affect the final brightness temperature measurements will be presented.

The most important effect of side lobes is related to the geometry of the instrument scan and its relationship to what is viewed below. Due to the curvature of the earth, the practical limit on the angle from which the earth's surface can be viewed from the height of the TIROS-N orbit is 61.6°, beyond which open space (radiating at 2.7 K) will be viewed. At the extreme MSU scan positions (1 and 11), the scan angle is 47.35°. Thus, side lobes beyond 14.25° will be sensing space. If the distribution of instrument side lobes is symmetric about the center point of the microwave footprint (such as the idealized SCAMS distribution in Fig. 2), the side lobe effect will also be symmetric. If side lobes are more prevalent to one side of the orbit than the other (such as the left side for TIROS-N in Fig. 2), however, that side will produce colder brightness temperatures at the more extreme scan angles since a greater proportion of the signal will be emanating from space. By weighting the response function by the area viewed at a particular angle relative to the axis of the cone being sampled by the instrument, the fraction of the response viewing space can be determined as a function of scan position. These fractions are given in Table 1 for the true TIROS-N MSU pattern and the idealized (SCAMS) antenna pattern used in developing the TIROS-N limb correction coefficients. The maximum TIROS-N value is 0.39% at position 1. While this is a small percentage,

TABLE 1. Percent of signal viewing space.

Scan position	From MSU (%)	From SCAMS (%)
1	0.39	0.32
2	0.28	0.20
3	0.10	0.13
4	0.01	0.09
5	0.00	0.06
6	0.00	0.02
7	0.00	0.06
8	0.00	0.09
9	0.02	0.13
10	0.04	0.20
11	0.06	0.32

its effect can decrease the measured brightness temperature by as much as 1.0 K.

The results using the observed MSU brightness temperatures without limb correction begin in Fig. 7. Two different simulation models were employed. The calculated brightness values used to derive the bias differences shown in Figs. 7a and 7c were produced from a simple simulation model that used the transmittance profile valid for the center point of each scan location. In contrast, the simulation used to derive Figs. 7b and 7d was more complex, employing an effective transmittance profile derived by subdividing the microwave footprint into separate solid angle elements, and weighting the transmittance from each element by its solid angle and antenna pattern value. An efficient method used to determine the effective transmittances in the side lobe corrections is presented in the Appendix.

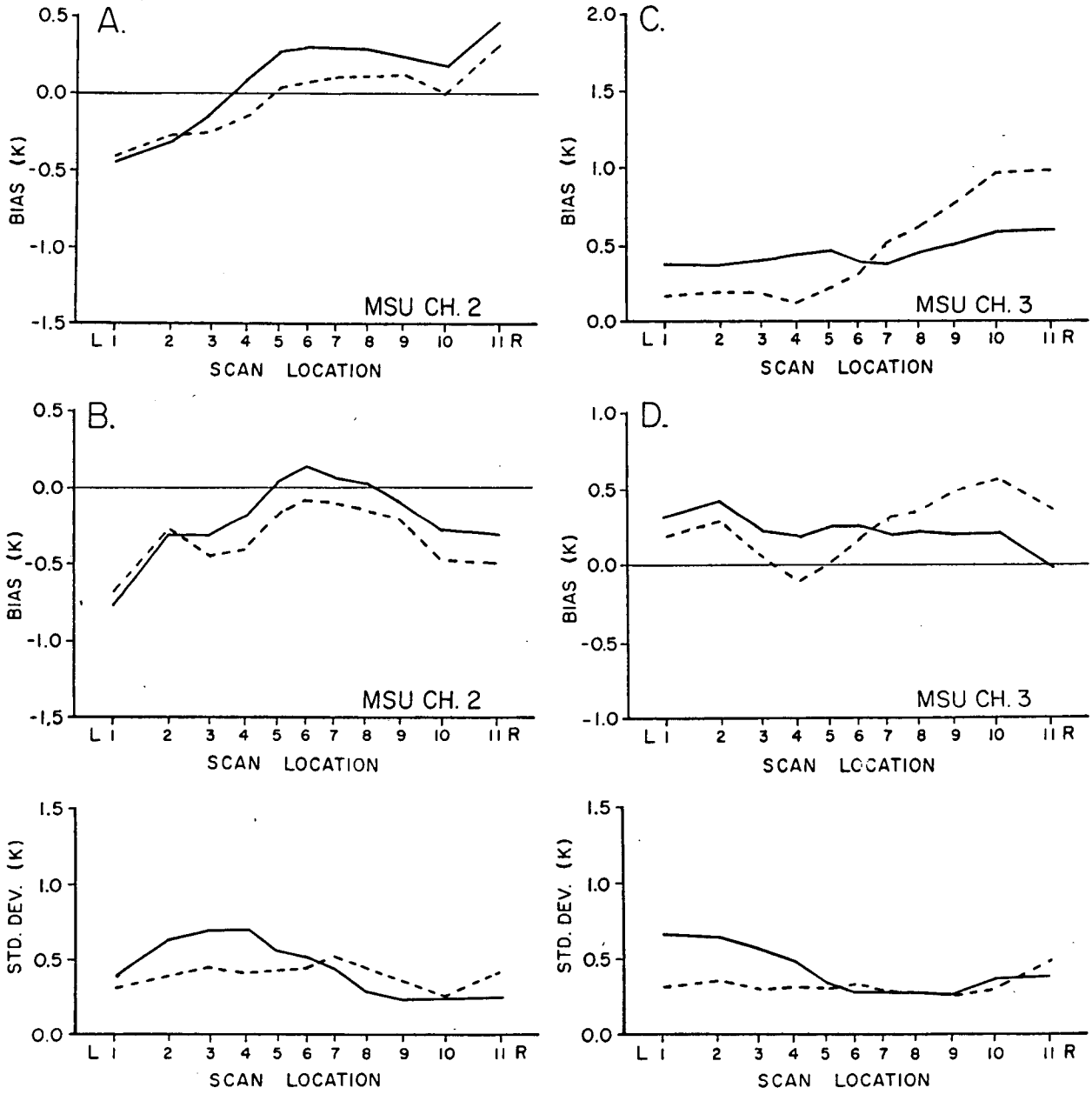

FIG. 7. Brightness temperature difference statistics for the observations without limb correction. Panels (A) and (C) use the standard NESDIS transmittance functions and the scan angle at the center of the MSU footprint, while panels (B) and (D) were derived from the antenna response weighted transmittances. Only one set of standard deviations are shown, because they were nearly identical for the two transmittance models.

The MSU Ch. 2 biases from the simpler simulation (Fig. 7a) exhibit a clear scan angle dependence, with the position 1 values nearly 1 K colder than those for position 11. This left-to-right bias is removed in results from the more complex simulation (Fig. 7b), with the difference biases at both outer positions now 0.5 K colder than those at the center (position 6). The difference standard deviations from Ch. 2 for both sim-

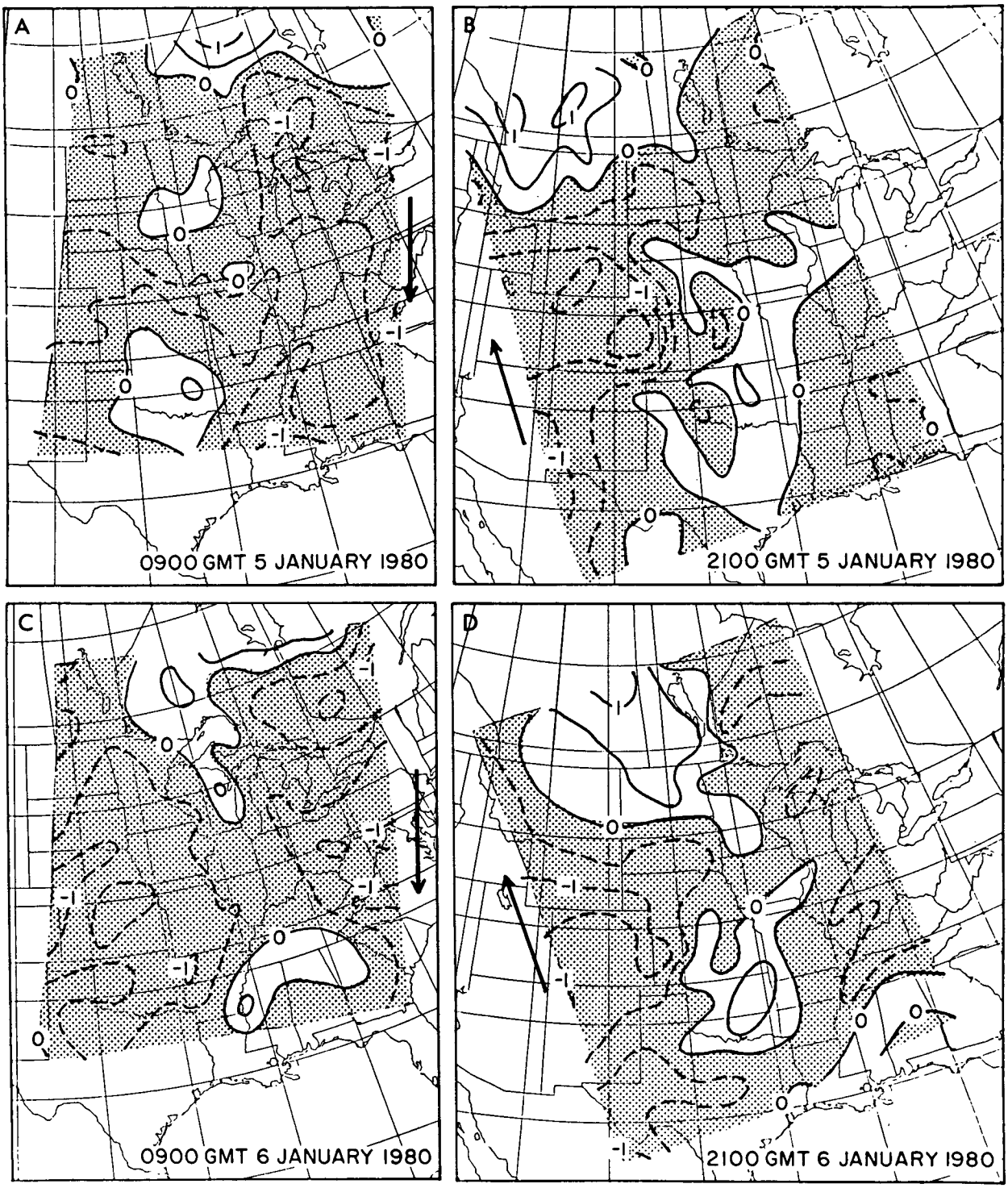

FIG. 8. Same as Fig. 5 except for brightness temperatures without limb correction and using the complex MSU antenna response function in the simulation.

ulations were nearly identical, and are illustrated in the panel beneath Figs. 7a and 7b. These values are substantially smaller than the limb-corrected results in Fig. 6. The biases from both simulations without limb correction for Ch. 3 (Figs. 7b and 7d) also improve upon the Ch. 3 limb-corrected biases in Fig. 6b.

The horizontal distributions of the observed-minus-simulated differences for the complex limb simulation are presented in Fig. 8 for MSU Ch. 2. Gradients in the differences are considerably weaker than those shown in Fig. 4 from the limb-corrected comparisons, while positive differences of greater than 1°C remain along the northern edge of all four orbits. This effect is present in all four simulations, and may have entered from the model used to estimate the MSU transmittances.

7. Summary

Comparisons of TIROS-N MSU brightness temperatures, both observed and simulated from radiosonde data, have been presented. Simulations of the data before limb correction proved to be in closer agreement with measurements than those after. The results indicated left-to-right asymmetry in the observed-minus-simulated differences from TIROS-N limb-corrected data, which most probably arise from asymmetry in the TIROS-N MSU antenna side lobe pattern. This antenna asymmetry was not included in the derivation of the limb correction coefficients applied by NESDIS during the retrieval processing for the Global Weather Experiment. Asymmetry in the MSU limb-corrected brightness temperatures was recognized by NESDIS before the period of study, but additive corrections to the brightness temperatures based on comparisons over the tropics were not incorporated into the retrieval procedure until after the time period presented here (Grody 1984, personal communication).

Another interesting facet of the results is that Ch. 2 observed brightness temperatures are warmer than simulated values in the cold air found in the northern portions of the passes, consistent with the positive retrieval errors detected in these regions by Koehler et al. (1983) and Koehler et al. (1987). Nearly one-half of the operational retrievals produced over the case study region were cloudy path retrievals that are directly influenced by MSU Ch. 2 in the lower troposphere. Also, the cloud detection algorithm for the infrared channels depends heavily on the Ch. 2 brightness temperatures. Thus, the asymmetry problems noted in this paper can adversely affect the clear and partly cloudy path retrievals. Incorporating more accurate antenna pattern models (if available) into the limb correction procedure would probably remove much of the asymmetry problem, without having to statistically determine the additive asymmetry corrections after the satellite is in orbit, as in current practice. Since the bias curves for the complex comparison in Fig. 7 still exhibited a problem in the simulation, with the outer position differences being slightly colder than the center differences, however, explanations other than instrument asymmetry must also be considered.

Acknowledgments. I wish to thank everyone who helped in this endeavor, including Hal Woolf and Anthony Schreiner of the NESDIS Development Laboratory in Madison, Wisconsin, who extracted the MSU data from the TIROS-N archive tapes and produced the limb-corrected data. Thanks are also due Dr. Norman Grody of NESDIS who provided the TIROS-N antenna patterns. I wish to also thank Dr. Lyle Horn, Charles Seman, and Linda Whittaker for assisting in the preparation of the manuscript, and the reviewers for their many helpful comments. This work was performed at the University of Wisconsin–Madison with support from NOAA Grant NA81AA-D-00087.

APPENDIX

An Efficient Method for Determining the Effective Transmittance

The radiant energy measured by the MSU instruments emanates from a volume of the atmosphere, and the sensitivity of the instrument to the energy emitted from different locations within the MSU footprint is defined by the instrument response function, showed in Fig. 2 for the TIROS-N MSU Ch. 2 instrument. As noted in (2), the transmittance function is usually modeled using $\tau = \exp(-U \sec\theta)$, where U is equal to the integral in (2), and θ is the scan angle of the center point of the microwave footprint. To include the effects of the instrument response function in the radiance simulations, an effective transmittance profile can be determined in the following manner:

$$\tau_e(p) = \sum_{i=1}^{N} a_i \tau_i / \sum_{i=1}^{N} a_i = \sum_{i=1}^{N} a_i \exp[-\sec\theta_i U(p)] / \sum_{i=1}^{N} a_i. \quad \text{(A1)}$$

The conical measurement volume has been broken into i solid angle elements represented by a grid of angles relative to the axis of the cone and azimuth angles directed around the axis of the cone. (See appendix A in Koehler 1986a.) The weighting coefficient, a_i, is the product of the antenna response for grid cell i, and the solid angle contribution by the cell, which increases as the angle from the axis of the cone increases. The angle θ_i is the local zenith angle of the satellite measured from the earth's surface for the grid cell. The costs in applying Eq. (A1) explicitly would be prohibitive, considering that N exponentials would have to be computed at each retrieval level and for each MSU observation location. The exponentials in Eq. (A1) can be

expressed as a power series, however, allowing (A1) to be rewritten as follows:

$$\tau_\epsilon(p) = \left[\sum_{i=1}^{N} a_i - U\sum_{i=1}^{N} a_i \sec\theta_i + \frac{U^2}{2}\sum_{i=1}^{N} a_i \sec^2\theta_i + \cdots + \frac{(-U)^J}{J!}\sum_{i=1}^{N} a_i \sec^J\theta_i\right] \Big/ \sum_{i=1}^{N} a_i. \quad \text{(A2)}$$

Points viewing space are not included in the sum. The summations within the brackets do not vary as a function of pressure, and need only be computed once, for each of the 11 scan positions. The U factors must still be computed at each level for a given temperature and moisture profile. In this study, the power series was truncated at $J = 65$. The portion of the signal coming from space at a particular MSU scan location (Table 1) was computed by adding the a_i factors for the points viewing space (as determined from the surface zenith angle computation), divided by the sum of all factors for the entire footprint.

REFERENCES

Grody, N. C., 1983: Severe storm observations using the Microwave Sounding Unit. *J. Climate Appl. Meteor.*, **22,** 609–625.

Gruber, A., and C. D. Watkins, 1982: Statistical assessment of the quality of TIROS-N and NOAA-6 satellite soundings. *Mon. Wea. Rev.*, **110,** 867–876.

Koehler, T. L., 1986a: An evaluation of scan angle dependence in limb-corrected MSU brightness temperatures. Evaluation of Alternative Retrieval Methods for TIROS-N and NOAA-6 Soundings. Final Rep., NOAA Grant NA81AA-D-00087, Dept. of Meteorology, University of Wisconsin–Madison, 65–93. [NTIS PB86 237005/AS.]

——, 1986b: High quality radiosonde-derived temperature and thickness data for alternative satellite retrieval experiments. Evaluation of Alternative Retrieval Methods for TIROS-N and NOAA-6 Soundings. Final Rep., NOAA Grant NA81AA-D-00087, Dept. of Meteorology, University of Wisconsin–Madison, 22–25. [NTIS PB86 237005/AS.]

——, and C. J. Seman, 1986: A modified version of the NESDIS TOVS Export Package for use in alternative retrieval method studies. Evaluation of Alternative Retrieval Methods for TIROS-N and NOAA-6 Soundings. Final Rep., NOAA Grant NA81AA-D-00087, Dept. of Meteorology, University of Wisconsin–Madison, 9–21. [NTIS PB86 237005/AS.]

——, J. C. Derber, B. D. Schmidt and L. H. Horn, 1983: An evaluation of soundings, analyses and model forecasts derived from TIROS-N and NOAA-6 satellite data. *Mon. Wea. Rev.*, **111,** 562–571.

——, C. J. Seman, J. P. Nelson III and L. H. Horn, 1987: An evaluation of alternatives to the retrieval methods used in processing FGGE Level II TIROS-N soundings. *J. Climate Appl. Meteor.*, **26,** 927–942.

LeMarshall, J. F., and A. J. Schreiner, 1985: Limb effects in satellite temperature sounding. *J. Climate Appl. Meteor.*, **24,** 287–290.

Phillips, N., L. McMillin, A. Gruber and D. Wark, 1979: An evaluation of early operational temperature soundings from TIROS-N. *Bull. Amer. Meteor. Soc.*, **60,** 1188–1197.

Schlatter, T. W., 1981: An assessment of operational TIROS-N temperature retrievals over the United States. *Mon. Wea. Rev.*, **109,** 110–119.

Weinreb, M. P., H. E. Fleming, L. M. McMillin and A. C. Neuendorffer, 1981: Transmittances for the TIROS Operational Vertical Sounder. NOAA Tech. Rep. NESS 85, U.S. Department of Commerce/NOAA/NESS, 60 pp.

Werbowetski, A., Ed., 1981: Atmospheric sounder users guide. NOAA Tech. Rep. NESS 83, U.S. Department of Commerce/NOAA/NESS, 82 pp. [NTIS PB81 230476.]